

Supporting Information

***In vivo* coating of bacterial magnetic nanoparticles by magnetosome expression of spider silk-inspired peptides**

Frank Mickoleit¹, Christian B. Borkner², Mauricio Toro-Nahuelpan^{1,3}, Heike M. Herold², Denis S. Maier¹, Jürgen M. Plitzko³, Thomas Scheibel^{2,4,5,6,7,8} & Dirk Schüler^{1*}

¹Dept. Microbiology / ²Dept. Biomaterials / ⁴Bayerisches Polymerinstitut (BPI) /
⁵Bayreuther Zentrum für Kolloide und Grenzflächen (BZKG) /
⁶Institut für Bio-Makromoleküle (bio-mac) / ⁷Bayreuther Zentrum für Molekulare
Biowissenschaften (BZMB) / ⁸Bayreuther Materialzentrum (BayMAT),
University of Bayreuth, D-95447 Bayreuth, Germany;
³Dept. Molecular Structural Biology, Max Planck Institute of Biochemistry,
D-82152 Martinsried, Germany

*Corresponding Author: Prof. D. Schüler

Department Microbiology, University of Bayreuth

Universitätsstraße 30, D-95447 Bayreuth, Germany

Tel.: +49-921-552728

Fax: +49-921-552727

E-mail: Dirk.Schueler@uni-bayreuth.de

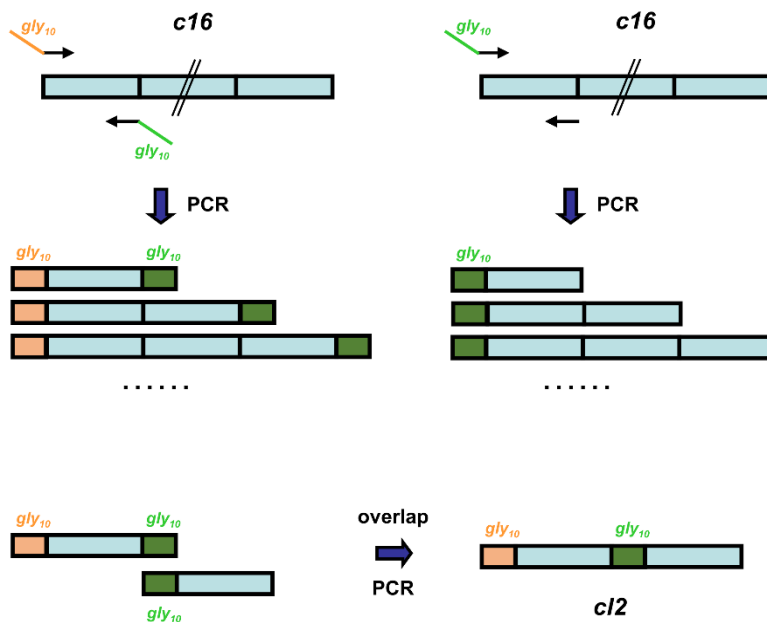


Figure S1. Scheme illustrating the construction of the *c12* spider silk gene fusion. *c1* units were generated by PCR and fused via overlap splicing, with a *gly*₁₀ linker (composed of ten glycine residues) connecting both units.

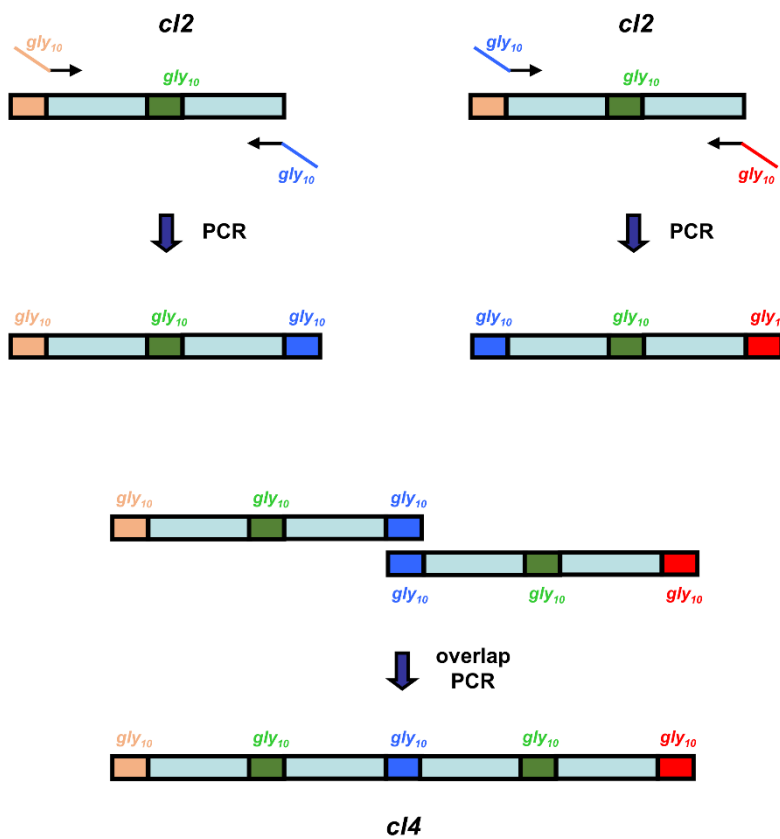


Figure S2. Scheme illustrating the generation of the *c14* spider silk gene. *c12* units were amplified by PCR and fused via overlap splicing, with a *gly*₁₀ linker (composed of ten glycine residues) connecting both units.

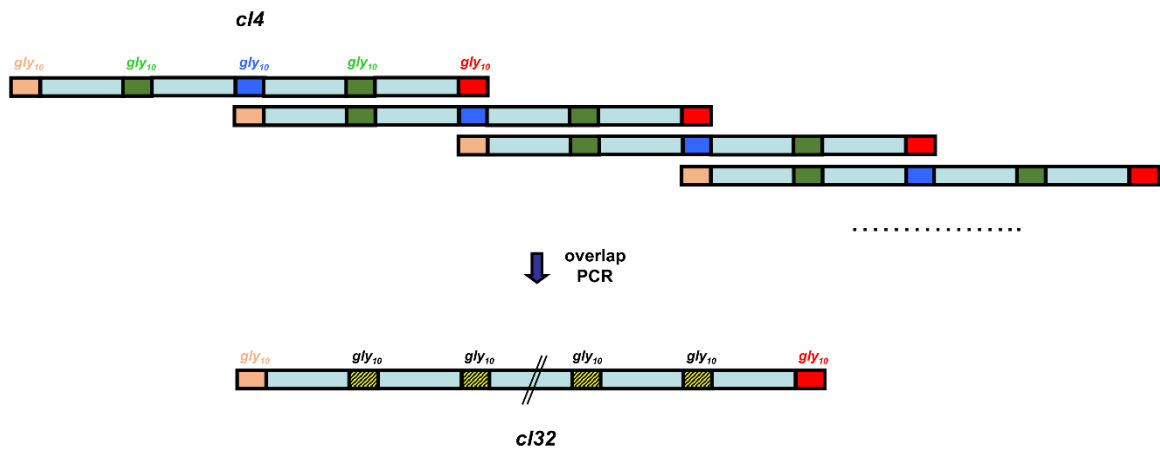


Figure S3. Construction of the *c132* spider silk gene fusion. *c14* units were fused via overlap splicing thereby generating fragments of different sizes, including the *c132* gene fusion.

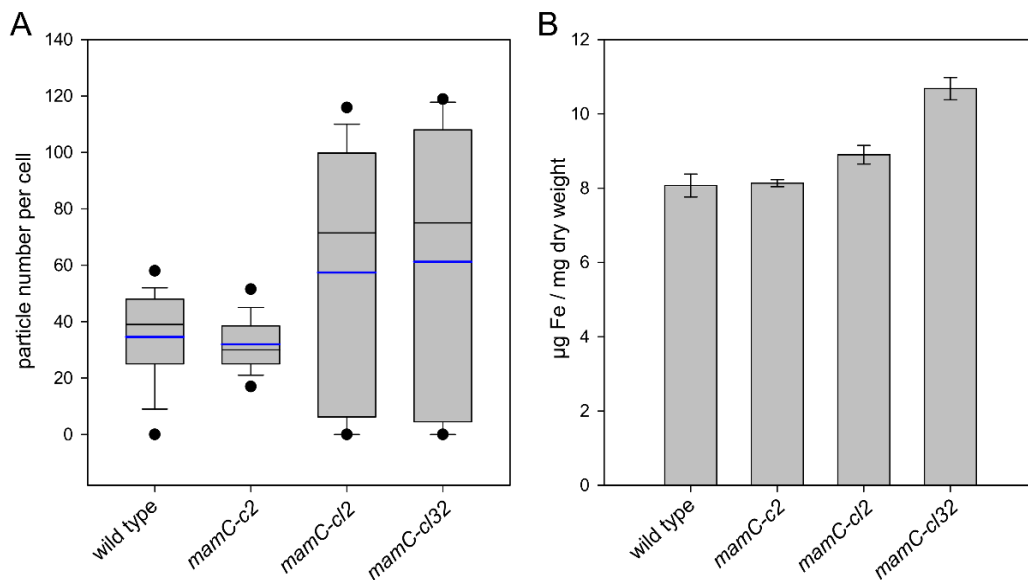


Figure S4. (A) Box plot illustrating magnetosome numbers per cell ($n = 285$) for the indicated *M. gryphiswaldense* strains. The boundary of each box closest to zero indicates the 25th percentile, a black line within the boxes mark the median, and the boundary of the boxes farthest from zero indicates the 75th percentile (50% central data). Whiskers above and below the boxes indicate the 90th and 10th percentiles. Outlying points represent the 95th and 5th percentiles, blue lines indicate the mean value. Whereas *mamC-c2* synthesized wild type-like amounts of magnetosomes (*mamC-c2*: 32 ± 11 ; wild type: 35 ± 16) arranged in one or two chains positioned ad midcell, total particle numbers were increased for *mamC-cl2* and *mamC-cl32* by 66% and 71%, respectively, with up to 60 magnetosomes per cell on average. (B) Iron contents (given as $\mu\text{g Fe}$ per mg cell dry weight) of strains *mamC-c2*, *mamC-cl2*, *mamC-cl32*, and the wild type of *M. gryphiswaldense*. For cells of the wild type and strain *mamC-c2*, similar iron contents were obtained, whereas for *mamC-cl2* and *mamC-cl32* cells the number of synthesized particles and the iron contents were significantly increased (10% for *mamC-cl2* and 32% for *mamC-cl32*), which is in accordance with the particle (mis)distribution visible by transmission electron microscopy.

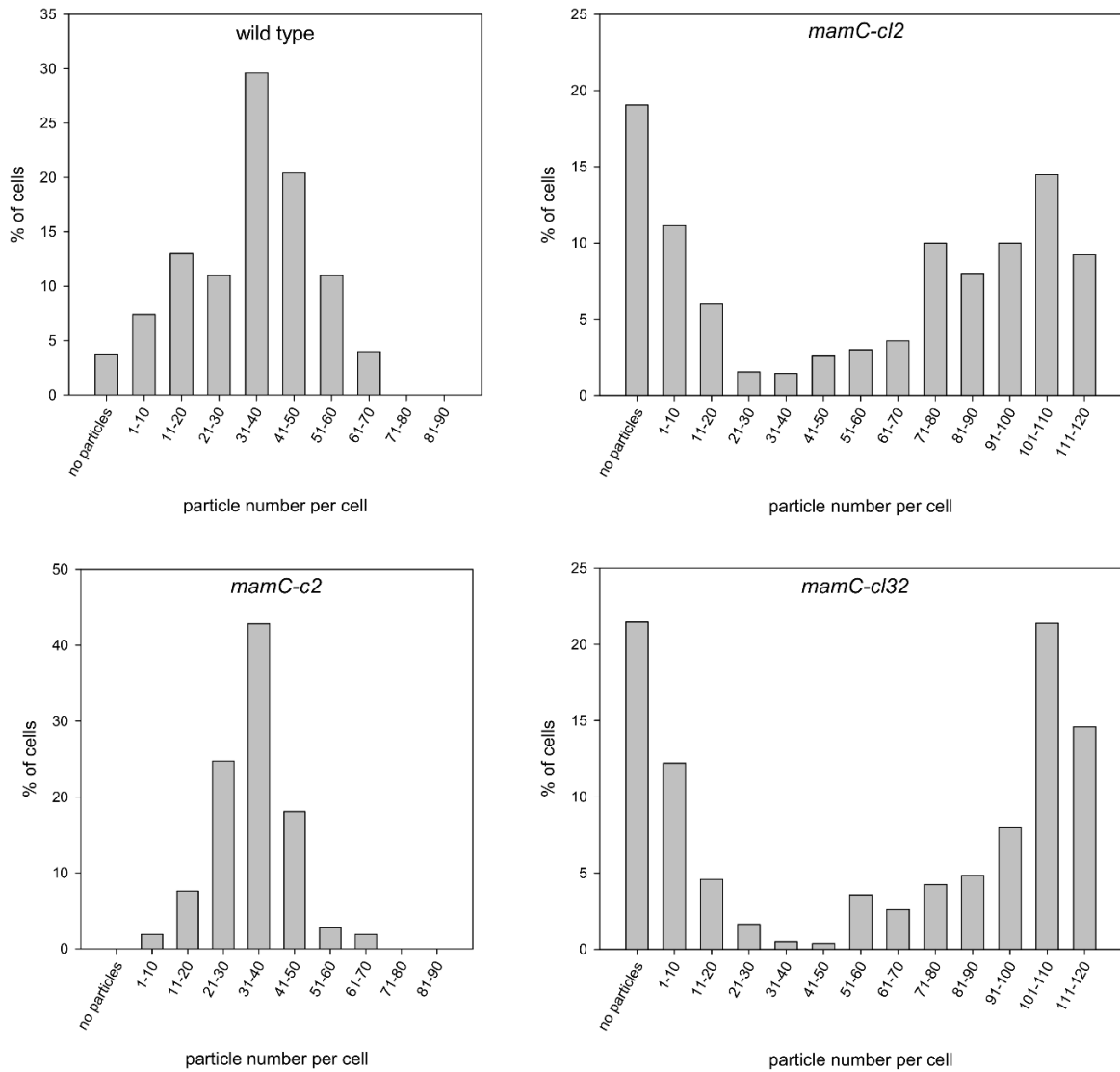


Figure S5. Magnetosome distribution of the spider silk motif expressing strains *mamC-c2*, *mamC-cl2* and *mamC-cl32*, and the wild type. The particle numbers per cell are given as percentage of the total amount of cells that were analyzed (n = 285). The bar charts visualize the particle misdistribution in strains *mamC-cl2* and *mamC-cl32*, with about 40% of the cells containing less than 20 particles, and about 50% containing more than 70 magnetosomes per cell. In contrast, cells of strain *mamC-c2* exhibit a wild type-like particle distribution.

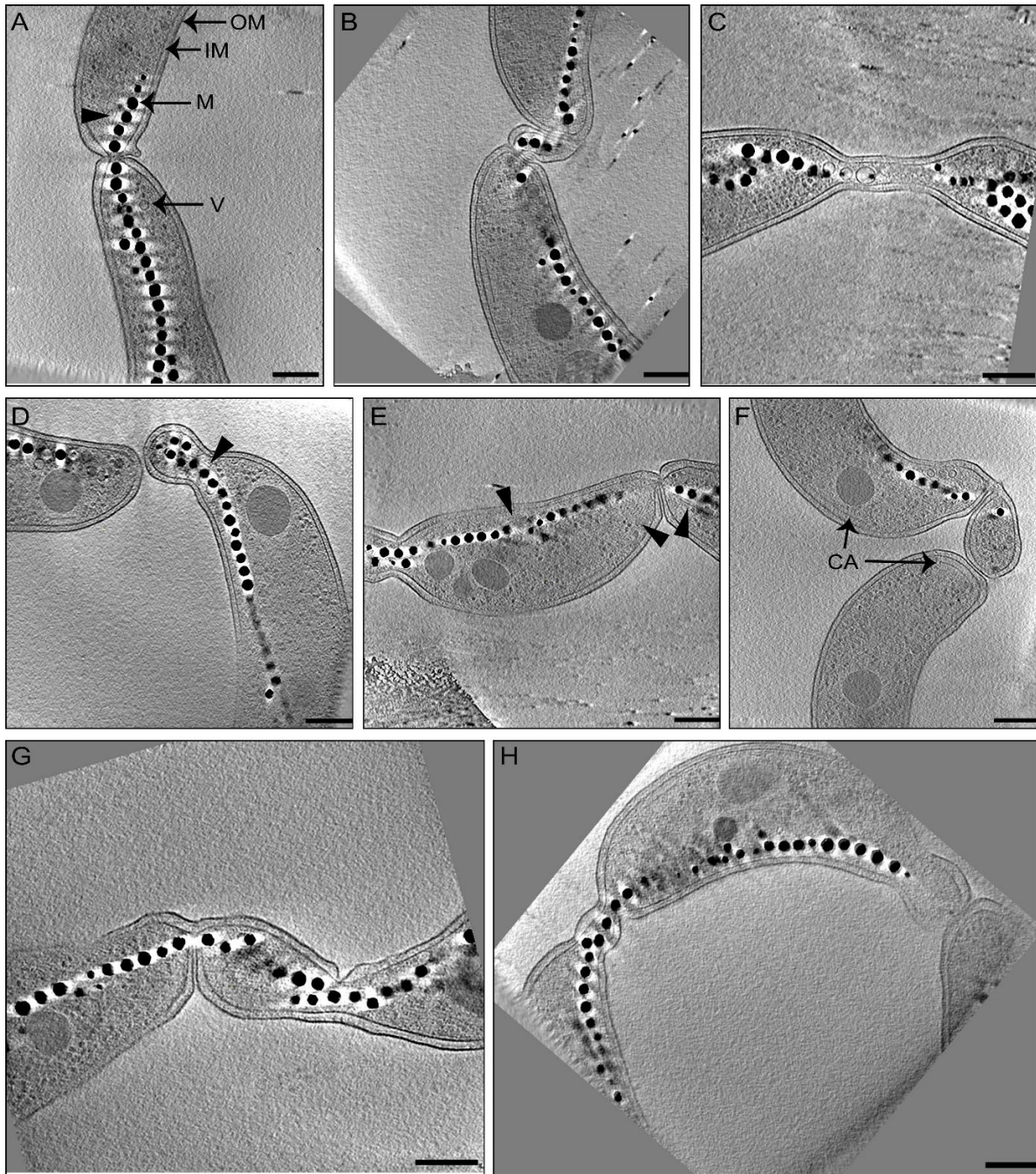


Figure S6. Cryo-electron tomography of *mamC-cl32* cells. (A-H) 12.8 nm thick slices (average of 5 slices) through the tomograms of cells undergoing cell division (n = 11). Cells display impairment in cytokinesis generating bridges of minicells due to improper cell division. (E) and (H) show slices from tomograms of bridging minicells. CA: chemoreceptor array, M: magnetite crystal, OM: outer membrane, IM: inner membrane, V: vesicle. Arrowheads indicate the presence of MamK filaments. Scale bars: 200 nm.

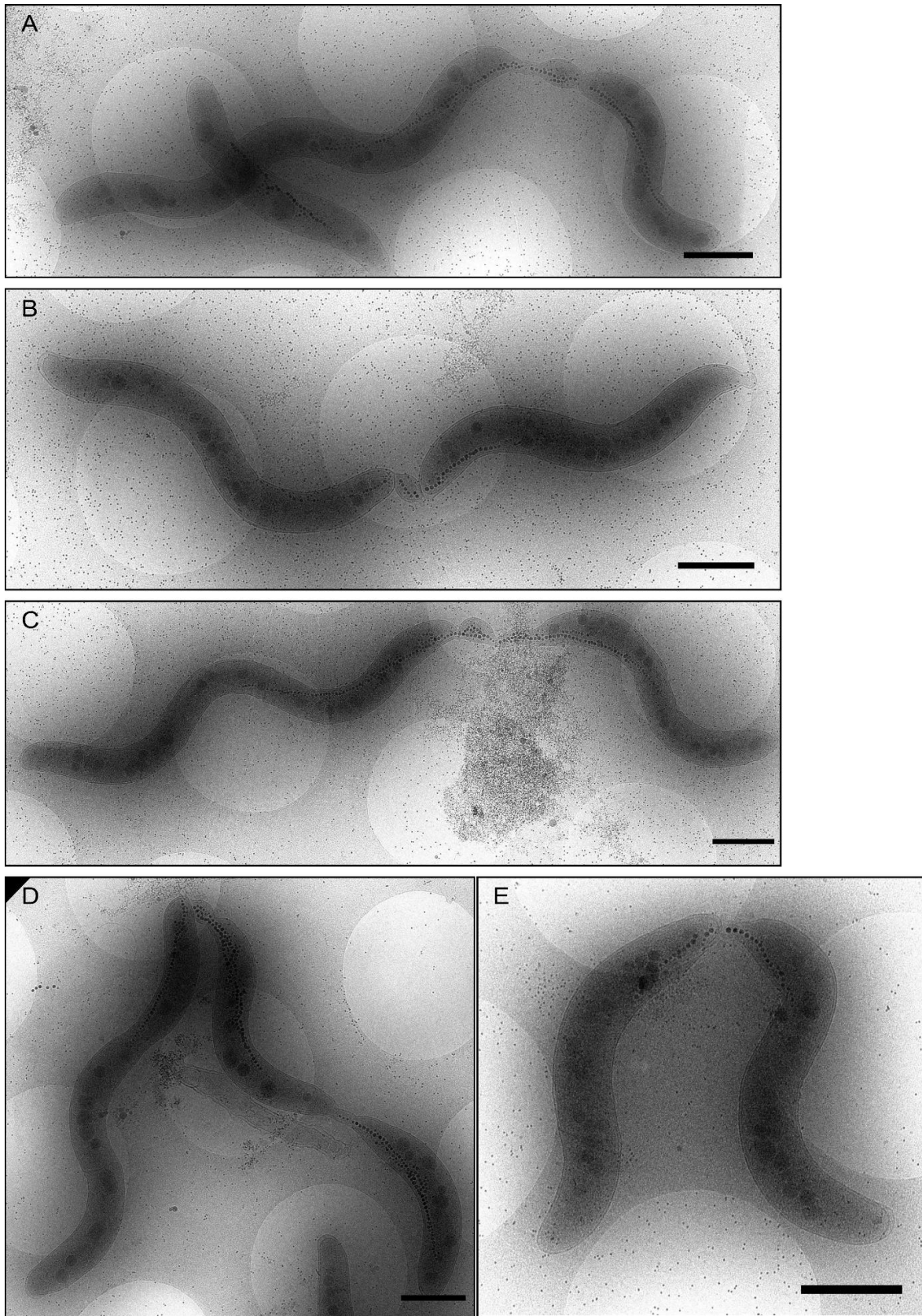


Figure S7. Overview of *mamC-cl32* strain by cryo-electron microscopy. (A-E) Cryo-electron micrographs depicting a conspicuous cell division defect present in the *mamC-cl32* strain. Scale bars: 1 μm.

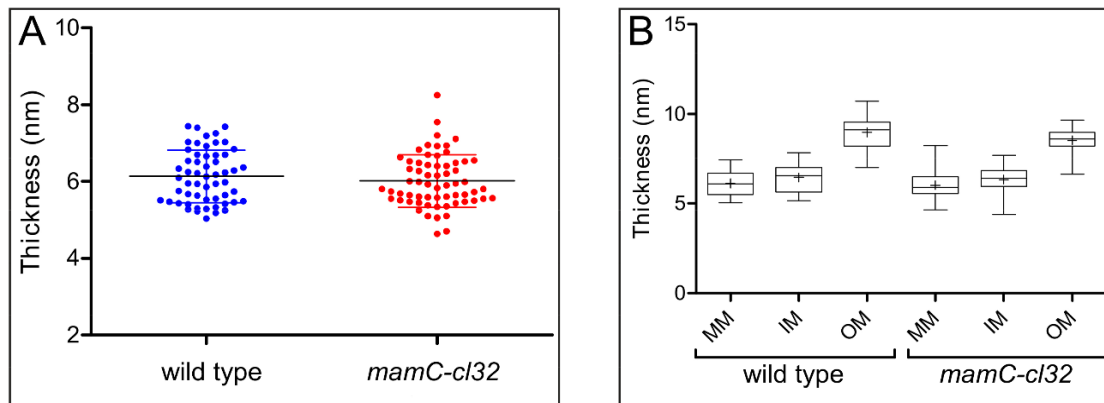
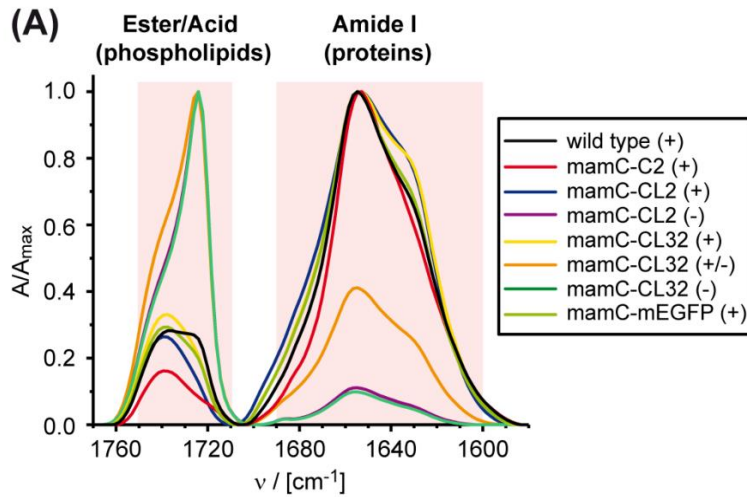


Figure S8. Magnetosome membrane thickness determined by cryo-electron tomography. Non-magnetic cells of the wild type (n = 9) and *mamC-cl32* (n = 11) were cultivated in low-iron medium to evaluate magnetosome vesicle (magnetosome membrane) thickness. (A) Dot plot of magnetosome membrane thickness of the wild type and *mamC-cl32* strains. The line represents the average and the bars the standard deviation. (B) The thickness of the magnetosome membrane as well as the inner (cytoplasmic) and outer membranes were quantified in the wild type and *mamC-cl32* strains. The boxes encompass from the 25th to 75th percentiles (50% central data). The line inside the box represents the median and the cross the average. The whiskers display the minimum and maximum values. MM: magnetosome membrane (vesicle), IM: inner membrane, OM: outer membrane.



(B)

entry	sample	$A_{\text{norm.}}(\text{amide I}) / A_{\text{norm.}}(\text{phospholipids})$
1	mamC-wt (+)	3.54
2	mamC-C2 (+)	6.19
3	mamC-CL2 (+)	3.77
4	mamC-CL2 (-)	0.11
5	mamC-CL32 (+)	3.02
6	mamC-CL32 (+/-)	0.41
7	mamC-CL32 (-)	0.10
8	mamC-mEGFP (+)	3.41

Figure S9. Representative normalized FTIR absorption spectra of magnetosome samples showing bands in the C=O stretch vibration regime. (A) C=O stretch vibration adsorption bands of phospholipid portion (esters, acids; $\sim 1750\text{-}1710 \text{ cm}^{-1}$) and protein portion (amide I; $\sim 1690\text{-}1600 \text{ cm}^{-1}$) of MamC-CL2 and MamC-CL32 magnetosomes for quality control measurements. (B) Protein-to-phospholipid ratios of different fermentation batches and constructs calculated from phospholipid and amide I band maxima ($A_{\text{norm.}}(\text{amide I})/A_{\text{norm.}}(\text{phospholipids})$) can be used for qualitative and empirical batch characterization. (+) high protein-to-phospholipid ratio (> 3); (+/-) intermediate protein-to-phospholipid ratio ($0.2 - 3$); (-) low protein-to-phospholipid ratio (< 0.2).

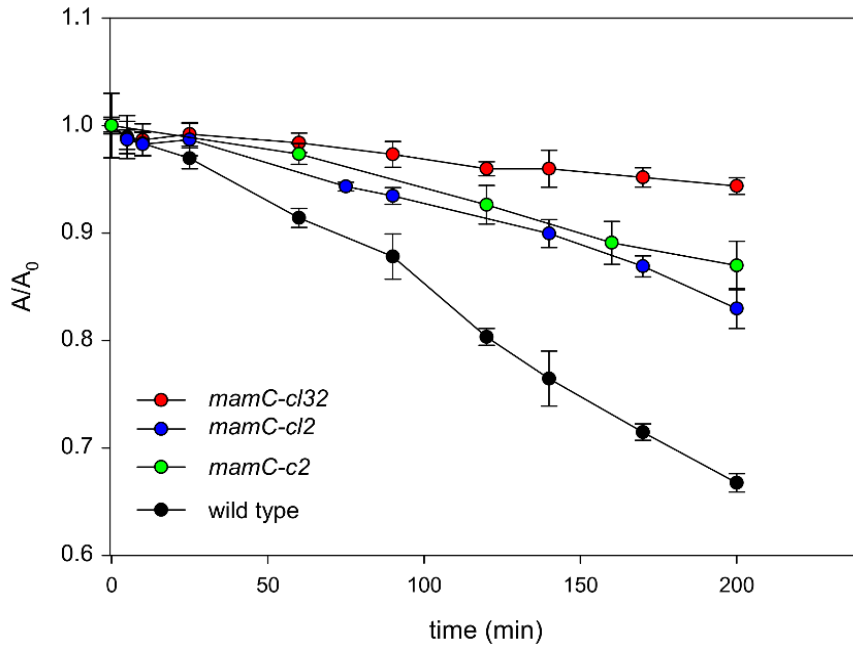


Figure S10. Normalized absorption values reflecting the sedimentation behavior of spider silk coated magnetosomes. Isolated particles of spider silk motif expressing strains *mamC-c2*, *mamC-cl2* and *mamC-cl32* and from the wild type were subjected to sedimentation assays. Sedimentation profiles are given as function of time and were normalized with the absorption at the initial time of the experiment. Standard deviations are based on at least three independent measurements.

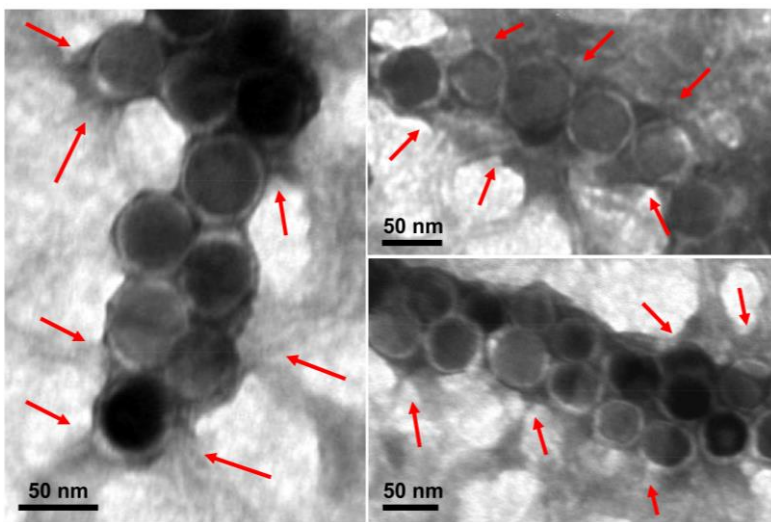


Figure S11. Assembly of nanofibrils in the presence of MamC-C2 magnetosomes. Isolated particles were incubated with 20 μ M freshly dialyzed eADF4(C16) monomers in potassium phosphate buffer. In TEM micrographs, fibril-like structure were visible at the particle surface (indicated by arrows), suggesting directed fibril growth by C2 triggered docking of further eADF4(16) monomers.

Table S1. Strains used in this study

Strain	Description	Source or reference
<i>Escherichia coli</i>		
DH5 α	F' <i>supE44</i> Δ <i>lacU169</i> (Φ 80 <i>lacZDM15</i>) <i>hsdR17 recA1</i> <i>endA1 gyrA96 thi-1 relA1</i>	Invitrogen
WM3064	<i>thrB1004 pro thi rpsL hsdS</i> <i>lacZ</i> Δ <i>M15 RP4-1360</i> Δ (<i>araBAD</i>)567 Δ <i>dapA1341::[erm pir]</i>	Metcalf, unpublished
<i>Magnetospirillum gryphiswaldense</i>		
<i>M. gryphiswaldense</i> MSR-1 R3/S1	Rif ^R , Sm ^R spontaneous mutant, lab strain	Schultheiss and Schüler 2003
<i>M. gryphiswaldense mamC-megfp</i>	R3/S1 Km ^R , transposon mutant with inserted <i>mamC-megfp</i> from P _{mamDC45}	Borg et al. 2014
<i>M. gryphiswaldense</i> MSR-1 IK-1	R3/S1 Δ <i>recA</i>	Kolinko et al. 2011
<i>M. gryphiswaldense mamC-c2</i>	R3/S1 Δ <i>recA</i> , Km ^R , transposon mutant with inserted <i>mamC-c2</i> from P _{mamDC45}	this study
<i>M. gryphiswaldense mamC-cl2</i>	R3/S1 Δ <i>recA</i> , Km ^R , transposon mutant with inserted <i>mamC-cl2</i> from P _{mamDC45}	this study
<i>M. gryphiswaldense mamC-cl32</i>	R3/S1 Δ <i>recA</i> , Km ^R , transposon mutant with inserted <i>mamC-cl32</i> from P _{mamDC45}	this study

Table S2. Plasmids used in this study

Plasmid name	Description	Source or reference
pCS-eADF4(C2)	Amp ^R , f1_origin, pBR322_origin, <i>c2</i> sequence	Huemmerich et al. 2004
pCS-eADF4(C16)	Amp ^R , f1_origin, pBR322_origin, <i>c16</i> sequence	Huemmerich et al. 2004
pBAM1	Km ^R , Amp ^R , oriR6K, <i>tnpA</i>	Martinez-Garcia et al. 2011
pSB9	pBAM1 with P _{mamDC45} , <i>mamC-gusA</i> , Km ^R , Amp ^R	Borg, unpublished
pFM-C2	pBAM1 with P _{mamDC45} , <i>mamC-c2</i> , Km ^R , Amp ^R	this study
pFM1	pBAM1 with P _{mamDC45} , <i>mamC-cl2</i> , Km ^R , Amp ^R	this study
pFM2	pBAM1 with P _{mamDC45} , <i>mamC-cl32</i> , Km ^R , Amp ^R	this study

Table S3. Primers and oligonucleotides used in this study. Restriction sites indicated in bold.

Primer name	Sequence (5' - 3')	Restriction site
linker1-sps fwd	GAATTGGC CCATGG AGGCGGAGGCGGTGGCGGAGGTGG CGGA ATCGAT GGTCTAGCGCGGCTGCAGCCGCGGC	NcoI / ClaI
sps-linker2 rev	GCCGCGCTAGAACCGCCACCGCCACCTCCGCGCCACCTC CACCGCCCGGACCGCCAGGACCGTAGCC	
linker2-sps fwd	CCGGGCGGTGGAGGTGGCGGGCGGAGGTGGCGGTGGCGGT TCTAGCGCGGCTGCAGCCGCGGCAGCTGCGTCCGCGCC	
sps-linker3 rev	GCCGCGCTAGAACCGCCACCTCCTCCGCCACCTCCTCCGCCAC CGCCGCCCGGACCGCCAGGACCGTAGCC	
linker3-sps fwd	CCGGGCGGGCGGTGGCGGAGGAGGTGGCGGAGGAGGTGGT TCTAGCGCGGCTGCAGCCGCGGCAGCTGCGTCCGCGCC	
sps-linker4 rev	GCCGCGCTAGAACCGCCACCTCCTCCGCCACCTCCTCCGCCAC CGCCGCCCGGACCGCCAGGACCGTAGCC	
sps rev	GGGACCC GGATCC TTAGCCCGGACCGCCAGGACCGT AGCC	SanDI / BamHI

Table S4. Particle size and layer thickness of magnetosomes isolated from *mamC-c2*, *mamC-cl2* and *mamC-cl32* mutant strains. Wild type and MamC-mEGFP magnetosomes (Borg et al. 2014) were used as controls. Particle diameters were determined by TEM (n = 150) and zetasizer measurements. For the latter, the theory of Smoluchowski was used to calculate overall diameters (Spiess et al. 2010). Particle sizes were analyzed in 10 mM HEPES/ 1 mM EDTA at pH 7.2. A one-way ANOVA test and a post-hoc Tukey test (using the wild type as control) confirmed that the overall difference between overall diameter means is statistically significant ($P < 0.05$).

Strain	Overall diameter (nm)		Diameter magnetite core (TEM) (nm)	Thickness of capsule (TEM) (nm)
	TEM	Zetasizer		
wild type	38.1 ± 7.3	40.7 ± 4.1	34.9 ± 5.7	5.2 ± 1.4
<i>mamC-megfp</i>	39.7 ± 8.1	41.2 ± 7.2	38.4 ± 6.2	4.3 ± 2.1
<i>mamC-c2</i>	52.6 ± 6.4	59.8 ± 6.9	40.1 ± 7.3	11.2 ± 3.8
<i>mamC-cl2</i>	56.8 ± 9.6	61.9 ± 5.7	45.9 ± 7.1	10.9 ± 2.5
<i>mamC-cl32</i>	50.6 ± 9.4	63.5 ± 5.8	39.4 ± 4.3	11.2 ± 4.3

References Supporting Information

- (1) Schultheiss, D.; Schüler, D. Development of a Genetic System for *Magnetospirillum gryphiswaldense*. *Arch. Microbiol.* **2003**, *179*, 89-94.
- (2) Borg, S.; Hofmann, J.; Pollithy, A.; Lang, C.; Schüler, D. New Vectors for Chromosomal Integration Enable High-Level Constitutive or Inducible Magnetosome Expression of Fusion Proteins in *Magnetospirillum gryphiswaldense*. *Appl. Environ. Microbiol.* **2014**, *80*, 2609-2616.
- (3) Kolinko, I.; Jogler, C.; Katzmann, E.; Schüler, D. Frequent Mutations within the Genomic Magnetosome Island of *Magnetospirillum gryphiswaldense* are Mediated by RecA. *J. Bacteriol.* **2011**, *193*, 5328-5334.
- (4) Huemmerich, D.; Helsen, C. W.; Quedzuweit, S.; Oschmann, J.; Rudolph, R.; Scheibel, T. Primary Structure Elements of Spider Dragline Silks and their Contribution to Protein Solubility. *Biochemistry* **2004**, *43*, 13604-13612.
- (5) Martinez-Garcia, E.; Calles, B.; Arevalo-Rodriguez, M.; de Lorenzo, V. pBAM1: an All-Synthetic Genetic Tool for Analysis and Construction of Complex Bacterial Phenotypes. *Bmc Microbiol.* **2011**, DOI: 10.1186/1471-2180-11-38
- (6) Spiess, K.; Lammel, A.; Scheibel, T. Recombinant Spider Silk Proteins for Applications in Biomaterials. *Biosci.* **2010**, *10*, 998-1007.